Journal of Hazardous Materials 170 (2009) 1110–1118

Contents lists available at ScienceDirect

Journal of Hazardous Materials

journal homepage: www.elsevier.com/locate/jhazmat

Efficient decolorization of azo dye Reactive Black B involving aromatic fragment degradation in buffered Co^{2+}/PMS oxidative processes with a ppb level dosage of Co^{2+}-catalyst

Yao-Hui Huang, Yi-Fong Huang, Chun-ing Huang, Chuh-Yung Chen*

Department of Chemical Engineering, National Cheng Kung University, Tainan City, 701, Taiwan

ARTICLE INFO

Article history:
Received 23 December 2008
Received in revised form 20 April 2009
Accepted 19 May 2009
Available online 22 May 2009

Keywords:
Wastewater
Azo dye
Peroxymonosulfate
Radicals
Decolorization

ABSTRACT

In order to generate powerful radicals as oxidizing species for the complete decolorization and degradation of azo dye Reactive Black B (RBB) at near neutral pH (pH 6), homogeneous activation of peroxymonosulfate (Oxone: PMS) by the trace Co^{2+}-catalysts was explored. We not only took advantage of the high oxidation–reduction potential of produced hydroxyl and sulfite radicals but also an opportunity to oxidize RBB to less complex compounds with extremely low dosages, especially the ppb level of the Co^{2+}-catalyst (stoichiometric ratio: $[Co^{2+}]_0/[RBB]_0 = 1.7 \times 10^{-6}$–$1.7 \times 10^{-5}$; $[PMS]_0/[RBB]_0 = 8$–32). Anion effects and pH effects were also carried out and discussed to simulate an actual application such as that of a textile waste stream. Both the degradations of RBB and its derivative aromatic fragments were illustrated successfully at UV–visable absorptions of 591 and 310 nm, respectively, and the possible relationships between them were also proposed and discussed, based on the experimental results. The RBB degradation in this Co^{2+}/PMS oxidative process successfully formulated a pseudo-first-order kinetic model at an isothermal condition of 25 °C with or without different anions present. The initial rate and rate constant were calculated under different comparative conditions, and the results indicate that the activity of both RBB decolorization and its degradation are not obviously dependent on the PMS concentration, but rather are related to the Co^{2+} dosage.

1. Introduction

The azo dyes, characterized by having an azo group consisting of two nitrogen atoms (–N=N–), are the largest class of dyes used in the textile industry [1]. Inside the azo dyes, there is a wide variety of dyes, namely, acid, reactive, disperse, vat, metal complex, mordant, direct, basic and sulphur dyes. Among these, reactive azo dyes are the most frequently used. Therefore, in this work, we have selected dye Reactive Black B (RBB), one of the most commonly used reactive dyes for textile finishing, to be the target compound for simulation as a representative dye pollutant of industrial wastewaters.

Nowadays, biological treatment is not a complete solution to the wastewater pollution problem due to biological resistance characteristic of some reactive dyes. Hence, using resources such as Advanced Oxidation Processes (AOPs), like Fenton, electro-Fenton and photo-Fenton processes, could be a good option to treat and eliminate textile dyes [2]. These processes appear to have the capacity to completely decolorize and partially mineralize the textile industry dyes in a short reaction time, as has been indicated by some studies [1,3–5]. AOPs essentially involve the generation of •OH, a powerful and non-selective oxidant that can be produced in advance by different combinations of AOPs' reagents, such as Fenton's reagents (i.e. H_2O_2 and Fe(II,III)), and combinations of O_3 (or H_2O_2) with UV radiation and/or TiO_2, among others, for the destruction of various hazardous pollutants.

Although the long reaction time required (several days to months) common to biodegradation technologies can be avoided by the substitution of AOPs, powerful AOPs do not achieve the necessary mineralization, and certain amount of sludge is always discharged by some AOPs, especially Fenton processes [6–11], creating another problem worse than the degradation itself. Moreover, AOPs such as Fenton-type reactions are limited by low pH conditions ($pH_i < 4$) [2], and although pH can be expanded to the neutral region in the presence of iron ligands [12,13], additional amounts of additives are required, and the degradation efficiency is decreased.

Based on the above concerns, another competitive oxidation method of substitution, cobalt/peroxymonosulfate (Co^{2+}/PMS), was employed in this study not only to reach a decrement of reagents but also to avoid any energy consumption (i.e. the UV source or electric power) in other AOPs at a higher pH (≥7) [14]. The use of PMS, a type of (bi)sulfite, is due to the fact that it has a higher oxidizing potential (1.82 V) than H_2O_2 (1.76 V) and intervenes in

* Corresponding author. Tel.: +886 6 2757575x62643; fax: +886 6 2360464.
E-mail address: ccy7@ccmail.ncku.edu.tw (C.-Y. Chen).

0304-3894/$ – see front matter © 2009 Elsevier B.V. All rights reserved.
doi:10.1016/j.jhazmat.2009.05.091

degradation processes in a more efficient way than does persulfate ($S_2O_8^{2-}$) [15,16]. Moreover, metal-ion catalyses of PMS have been reported to generate the reactive oxidative radicals $HSO_5^{-\bullet}$, $SO_4^{-\bullet}$ and $^\bullet OH$, involving chain oxidative processes for the mineralization of organic pollutants [17,18]. Most importantly, the utilization of the Co^{2+}/PMS process in this study to oxidize RBB is due to the proposed premise that the $SO_4^{-\bullet}$ which is predominantly produced is powerful but is an organics-selective oxidant which is totally different from $^\bullet OH$ (non organics-selective) [19,20].

Therefore, the main objective of this study is to analyze the feasibility of decolorization and degradation of RBB by the use of Co^{2+}/PMS oxidative processes with such extremely low dosages of Co^{2+} ($[Co^{2+}] = 1–10\ \mu g\ L^{-1}$) and PMS (0.08–0.32 mM). Although low mineralization efficiency is the common drawback of a single use of sulfite–bisulfite–pyrosulfite systems, this low dosage Co^{2+}/PMS oxidative process is expected to be looked upon as a superior choice for a good pretreatment to selectively decompose the stubborn structures of benzenic and phenolic derivatives first. Achieving good mineralization is not the goal of this study, while facilitating the mineralization for the follow-up treatment of other AOPs through the efficient decomposition of derivative aromatic fragments of RBB using the pretreatment suggested in this Co^{2+}/PMS process is a good consideration and is interesting. Another significant benefit from this concept is to allow direct practice of the treatment of RBB, even in alkaline conditions ($pH \geq 7$). Furthermore, the influence of different operational parameters (pH, PMS dosage, Co^{2+} dosage, and the anion effects) which affect the efficiency of Co^{2+}/PMS processes in RBB oxidation was also investigated.

2. Experimental

2.1. Materials

Reactive dye-Black B (Fig. 1) was purchased from Aldrich. For reference, the structure of the reactive dye-Black B is displayed as the target dye used in all trials. Potassium peroxymonosulfate (PMS: OXONE®, DuPont) was purchased from Aldrich. Cobaltous sulphate was obtained from Showa. All salts of reagent grade for anion effect study, including sodium chlride (NaCl), sodium perchlorate ($NaClO_4$), potassium nitrate ($NaNO_3$), and disodium hydrogen phosphate dodecahydrate (Na_2HPO_4), were obtained from J.T.Baker, Showa, Riedel-de Haën, and Merck, respectively. Other chemicals used herein, including sulfuric acid, sodium hydroxide and the phosphate buffer solution (obtained from Scharlau), were of reagent grade and were used to adjust pH. All sample solutions were prepared using deionized water from the Millipore Milli-Q system.

2.2. Experimental procedures and analysis

Firstly, it is worth to be noted here that the target concentration of RBB was selected at 10 ppm in this study in order to simulate the actual effluent (and/or leakage) of textile industry; although RBB effluents can reach the allowed criteria of discharge (100 ppm) by photo/ferrioxalate technology [12], the color-problem of the effluent is still remained and unsolved. The metal-activation of PMS for all RBB degradation reactions was carried out in a batch reactor (jar-testing reaction) at atmospheric temperature (25 °C). RBB reactive solutions (0.01 mM (10 ppm)) were buffered with ~0.305 mM phosphate ($[KH_2PO_4] = 0.100$ mM and $[Na_2HPO_4] = 0.205$ mM) at pH 6 and/or adjusted by $NaOH_{(aq)}$ at different reaction pH for the pH effect study. All reactions were initiated by the simultaneous addition of the estimated amounts of PMS (0.08–0.32 mM) and Co^{2+} (1.7×10^{-4} mM–1.7×10^{-3} mM, i.e. 1–10 $\mu g\ L^{-1}$) in a thermostatic water bath. The volume of all reactive solutions was 1.0 L in each trial.

As unfavorable halogen ions such as Cl^- participate in the reaction, they simultaneously scavenge most of the radicals produced, thus generating chloride that may further transfer to $Cl_2(g)$ as a result of the combination of two chloride atoms [21,22]. Due to the study's requirement to clarify the kinetics of the RBB/PMS oxidation system, all the reagents, including an acid source for the purpose of adjusting the pH and a Co(II,III) sources required for activation, are frequently used in the sulfate form instead of the chloride form to avoid such unwanted scavengers, with the exception of the NaCl salt used for the anion effect study. In order to clarify the influence of anions on RBB removal during Co^{2+}/PMS oxidative processes, various salts (10 mM), including chloride, perchlorate, nitrate, and phosphate, were added.

The absorption of RBB is maximum at $\lambda_{max} = 591$ nm, and the color removal relating to its decomposition was determined using a UV–visible spectrophotometer. UV–visible spectra of all other species including derivative aromatic fragments were also obtained using a Hewlett–Packard 8453 diode array spectrophotometer (Agilent). All UV–visible spectra of the RBB oxidation were evaluated spectrophotometrically at $\lambda = 190–1100$ nm by subtracting a background value of the single mixture of Co^{2+}/PMS from total absorption automatically, and all RBB samples in the oxidation processes were analyzed immediately after sampling so as to prevent further reactions. Furthermore, almost no Co(II,III) ion residuals were found using the atomic absorption analysis during the degradation of RBB in all of the oxidation processes due to the use of extremely small amounts of $[Co^{2+}]_0$.

3. Results and discussion

3.1. Effect of pH

The pH of the solution controls the production rate of the radicals ($SO_4^{-\bullet}$ and $^\bullet OH$) and the concentration of Co^{2+}. Therefore, pH is an important parameter for this Co^{2+}/PMS process. The effect of pH on the decolorization of RBB by the Co^{2+}/PMS oxidative process is shown in Fig. 2. In the acidic range, the decolorization rate increases sharply as the solution pH increases from 3.5 to 5 in the Co^{2+}/PMS process; on the contrary, it decreases sharply as the pH of the solution increases from 6 to 8.4. Fig. 2b illustrates how as the percentage of decolorization overlapped at different pH within a 30 min period, the color removal increased from 3% to 25% at pH 3.5 and from 88% to 100% at pH 5. However, the largest variation occurred at pH 4, from 26% to 93%. When the reaction pH was higher than 5, the color removal decreased further, especially in alkaline conditions, from 99% to 85% at pH 6, 88% to 71% at pH 7, and 40% to

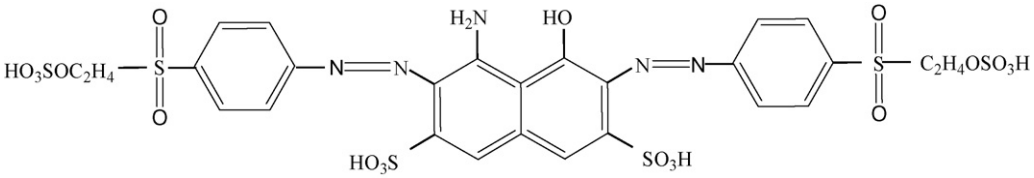

Fig. 1. Chemical structure of dye-Reactive Black B (RBB).

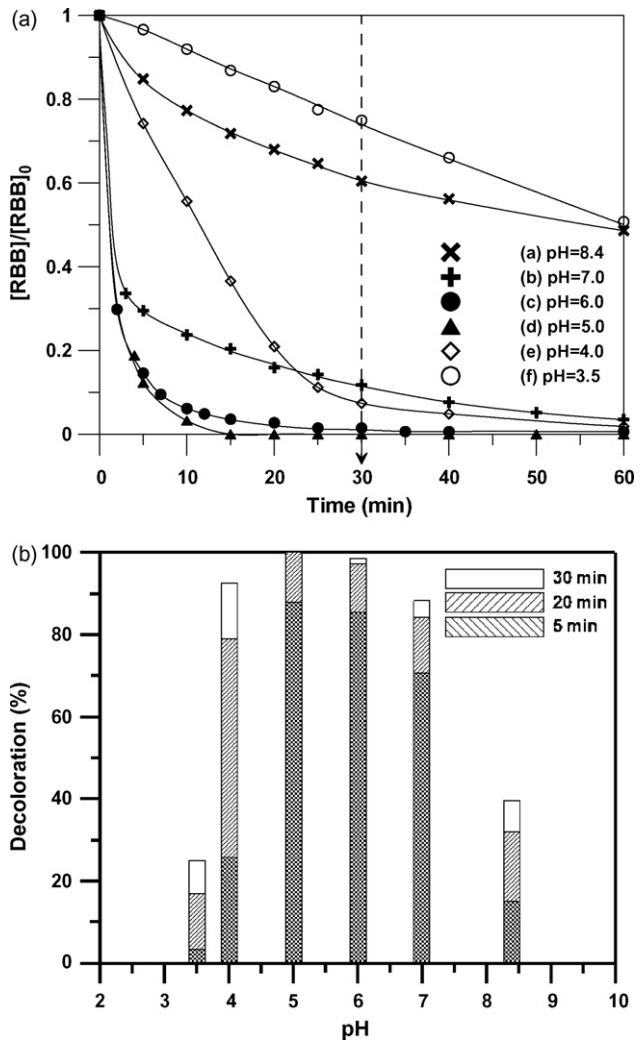

Fig. 2. Effect of pH on the RBB removal (a) and the corresponding percentage of RBB decolorization (b) by Co^{2+}/PMS processes. Experimental conditions: $[RBB]_0 = 0.01$ mM (10 ppm); $[Co^{2+}]_0 = 1.7 \times 10^{-3}$ mM (10 ppb); $[PMS]_0 = 0.16$ mM (100 ppm); reaction pH 6.0 (adjusted by $NaOH_{(aq)}$); reaction temperature = 25 °C.

15% at pH 8.4, respectively. Hence, the optimum pH was proposed to be about 5–6 for the RBB solution tested. In these processes, the decrease in decolorization at pH above 6 is probably due to the less reactivity of the Co^{2+} hydroxo complex (formed during the higher pH reaction) with PMS; and especially the proposed evidence that $SO_4^{-\bullet}$ (and/or $SO_3^{-\bullet}$) is rather stable in the acidic process ($pH \leq 5$) [14,23]. At a low pH, the removal rate is limited due to the H^+ ion scavenging effects of the radicals $^\bullet OH$ and $SO_4^{-\bullet}$. (Eq. (1)–(2)) [24].

$$^\bullet OH + H^+ + e^- \rightarrow H_2O \quad (1)$$

$$SO_4^{-\bullet} + H^+ + e^- \rightarrow HSO_4^{-\bullet} \quad (2)$$

3.2. Effect of Co^{2+} and PMS dosage

In order to determine the optimum initial PMS concentration, a set of experiments on RBB degradation was carried out within the 60 min Co^{2+}/PMS treatments of RBB at varying initial PMS concentrations presented in Fig. 3. The PMS concentrations were studied in the range of 0.08–0.32 mM (i.e. 50–200 ppm), and were progressively increased while maintaining the selected concentration of Co^{2+} constant at an extremely low value of 1.7×10^{-4} mM (1 ppb). All experiments were carried out for 60 min at an adjusted pH of 6. It is evident from Fig. 3 that the optimum PMS dosage was found

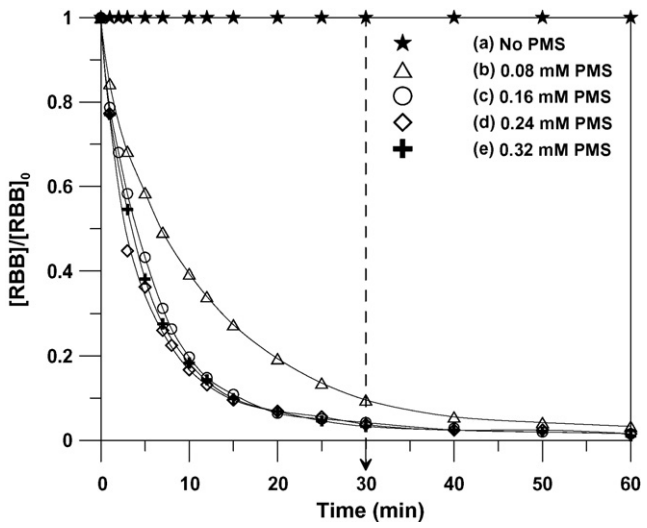

Fig. 3. Effect of PMS dosage on the removal of RBB by Co^{2+}/PMS processes. Experimental conditions: $[RBB]_0 = 0.01$ mM (10 ppm); $[Co^{2+}]_0 = 1.7 \times 10^{-4}$ mM (1 ppb); reaction pH 6.0 (adjusted by $NaOH_{(aq)}$); reaction temperature = 25 °C.

to be 0.16 mM (100 ppm) due to the fact that the RBB removal efficiency did not increase significantly even when the concentration of PMS was doubled (i.e. 0.32 mM (200 ppm)).

Correspondingly, the effect of the initial Co^{2+} concentration on the treatment efficiency of RBB was also investigated by trying different concentrations of Co^{2+} at the optimum PMS concentration previously determined to be 0.16 mM (100 ppm) at pH 6.0 (Fig. 4). The selected Co^{2+} concentration was in the range of 1.7×10^{-4}–1.7×10^{-3} mM (i.e. 1–10 ppb). Similarly, the optimum cobalt concentration was found to be 8.5×10^{-4} mM (5 ppb) due to the fact that the RBB removals did not increase significantly even when the concentration of Co^{2+} was doubled (i.e. 10 ppb).

It is interesting to mention here that although both the PMS-oxidant and the Co^{2+}-catalyst have an optimum concentration. Based on the use of an extremely low dosage of the Co^{2+}-catalyst, the ideal dosage of Co^{2+} for actual application is preferably 10 ppb, rather than 5 ppb, in order to ensure a sufficient amount of regenerated Co^{2+} (Eqs. (16)–(17)) to continuously activate 100 ppm PMS completely via the chain oxidative pathways suggested in Sec-

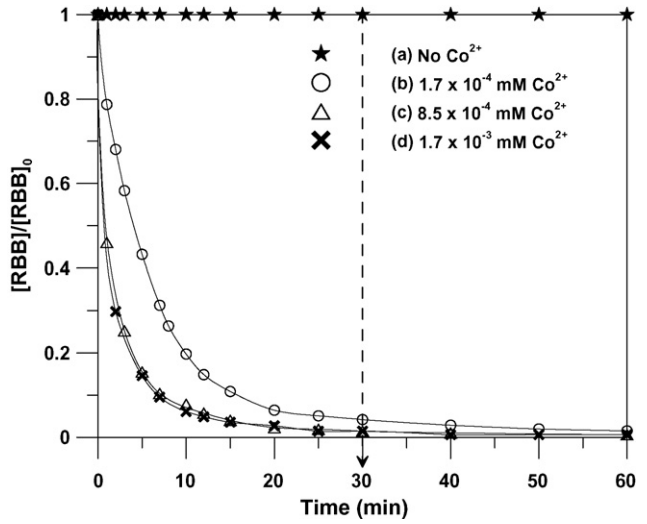

Fig. 4. Effect of Co^{2+}-catalyst dosage on the removal of RBB by Co^{2+}/PMS processes. Experimental conditions: $[RBB]_0 = 0.01$ mM (10 ppm); $[PMS]_0 = 0.16$ mM (100 ppm); reaction pH 6.0 (adjusted by $NaOH_{(aq)}$); reaction temperature = 25 °C.

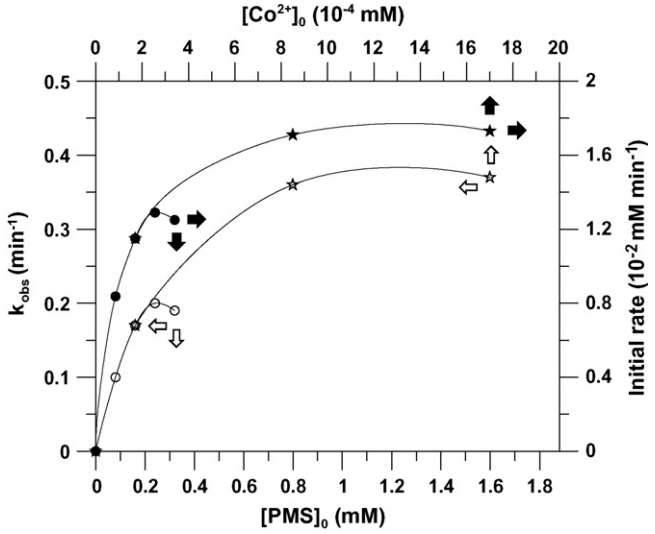

Fig. 5. Comparative plot of Initial rate and k_{obs} of RBB removal related to various dosages of Co^{2+}-catalyst and PMS oxidant. Experimental conditions: $[RBB]_0$ = 0.01 mM (10 ppm); reaction pH 6.0 (adjusted by $NaOH_{(aq)}$); reaction temperature = 25 °C. Initial rate calculation was defined within 5 min.

tion 3.6. Furthermore, the dark step of Co^{2+} regeneration via PMS has also been suggested by Anipsitakis and Dionysiou (2004) and Manivannan and Maruthamuthu (1987) [17,18]. Initial rate and rate constant (k_{obs}) indicate the comparative study of overall removal efficiencies obtained within 60 min treatments of RBB via Co^{2+}/PMS oxidative processes at varying initial PMS dosages or Co^{2+} concentrations which are summarized in Fig. 5 and Table 1. When a comparison of curve ☆ with curve ⋆ is made in Fig. 5, it can be seen that both the initial rate and the k_{obs} increased with increasing initial Co^{2+} concentrations, though they did not increase significantly when $[Co^{2+}]_0$ was greater than 8.5×10^{-4} mM (5 ppb). In comparison, the performance at varying initial PMS dosages was different from that at varying initial Co^{2+} dosages, as can be seen in curves ○ and ● of Fig. 5, which show that both the initial rate and the k_{obs} declined after an overdose of $[PMS]_0$ = 0.32 mM (i.e. 200 ppm). The above results as shown in Table 1 also indicate that the removal efficiencies of RBB within the select concentrations of reagents are not obviously dependent on the PMS concentration, but rather are related to the Co^{2+} dosage in a Co^{2+}/PMS process due to the extremely small $[Co^{2+}]$ variation of ppb level.

3.3. Effect of anions

This study also examined the effect of anions such as Cl^-, ClO_4^-, NO_3^-, and PO_4^{3-}, for which, due to the salts are usually found in textile waste streams, on the decolorization of RBB. In the absence of salt, the fast RBB decolorization was 94% at 10 min in the Co^{2+}/PMS oxidative process. In the presence of salt, shown in Fig. 6a, the RBB decolorization was 93% with 10 mM Cl^- addition, 97% with 10 mM ClO_4^- addition, 96% with 10 mM NO_3^- addition, and 84% with 10 mM PO_4^{3-} addition at 10 min, respectively. Though the addition of 10 mM PO_4^{3-} to the RBB dye solution caused a ~10% decrease in the decolorization percentage at 10 min, addition of these various kind of salts did not affect the removal rate significantly in a reaction time greater than 30 min, in which case there was almost complete bleaching. The positive effects of ClO_4^- and NO_3^-, especially ClO_4^-, may be due to the fact that active oxygen can be produced during the degradation of perchlorate [25], thus promoting the RBB removal efficiency. Contrarily, the small decrease in RBB removal efficiency at 10 min (~1%) in the presence of Cl^- was due to the scavenging effect of the chloride ion (Eqs. (3)–(4)) [26].

$$Cl^- + HO^\bullet \rightarrow HOCl^{-\bullet} \quad (3)$$

$$HOCl^{\bullet -} + H^+ \rightarrow Cl^\bullet + H_2O \quad (4)$$

It was interesting to discover that ~10% of RBB removal efficiency decreased at the same reaction time of 10 min in the presence of PO_4^{3-}. This may be also due to the fact that phosphate was believed to be a hydroxyl radical scavenger [27], indicating a more negative anion effect occurred in the case of this PO_4^{3-} species rather than that demonstrated with Cl^-.

Fig. 6b is fitted by a pseudo-first-order model (R^2 = 0.91–0.99), using the exponential regression analysis presented in Table 1, formulated from the original plot of the normalized remaining concentration ($[RBB]/[RBB]_0$) vs. reaction time (t) (Fig. 6a). All

Table 1
Kinetic rate constants of Co(II)-activated PMS oxidation of 0.1 mM RBB in NaOH-controlled solutions (pH 6) (Part 1) and/or in anion-effected solutions (pH 6) (Part 2) at 25 °C.

Part (1)							
Run	[Co(II)] (10^{-4} mM)[a]	[PMS] (mM)[b]	Initial rate (mM min^{-1})[c]	RBB decay of R_i (%)[d]	$t_{1/2}$ (min)[f]	k_{obs} (min^{-1})[e]	R^2 of k_{obs}
1	1.7(1 ppb)	0.16	1.15×10^{-2}	57	3.95	0.17	0.99
2	8.5(5 ppb)	0.16	1.71×10^{-2}	85	0.94	0.36	0.89
3	17(10 ppb)	0.16	1.73×10^{-2}	85	0.86	0.37	0.91
4	1.7(1 ppb)	0.08	8.37×10^{-3}	41	6.24	0.10	0.98
1	1.7(1 ppb)	0.16	1.15×10^{-2}	57	3.95	0.17	0.99
5	1.7(1 ppb)	0.24	1.29×10^{-2}	64	2.65	0.20	0.99
6	1.7(1 ppb)	0.32	1.25×10^{-2}	62	3.74	0.19	0.99

Part (2) Run	Anion[g]	Initial rate (mM min^{-1})[c]	RBB decay of R_i (%)[d]	$t_{1/2}$ (min)[f]	k_{obs} (min^{-1})[e]	R^2 of k_{obs}
3	Blank (non anion add)	1.73×10^{-2}	85	0.86	0.37	0.91
7	PO_4^{3-}	1.36×10^{-2}	67	2.59	0.22	0.96
8	NO_3^-	1.70×10^{-2}	84	2.08	0.36	0.99
9	ClO_4^-	1.76×10^{-2}	87	2.11	0.39	0.99
10	Cl^-	1.57×10^{-2}	77	2.23	0.31	0.99

[a] 1.7×10^{-4} mM ≃ 1 ppb; 8.5×10^{-4} mM ≃ 5 ppb; 17×10^{-4} mM ≃ 10 ppb.
[b] 0.08 mM ≃ 50 ppm; 0.16 mM ≃ 100 ppm; 0.24 mM ≃ 150 ppm; 0.32 mM ≃ 200 ppm.
[c] The initial rate was expressed by the decreased RBB concentration (ΔC) per minute (within first 5 min).
[d] R_i indicates the initial rate at first 5 min.
[e] k_{obs}(observed rate constant): The pseudo-first order kinetics constant for the oxidation of RBB by Co/PMS.
[f] Half-life time of RBB in Co/PMS oxidation process.
[g] $[Co(II)]_0 = 17 \times 10^{-4}$ mM ≃ 10 ppb; $[PMS]_0$ = 0.16 mM ≃ 100 ppm.

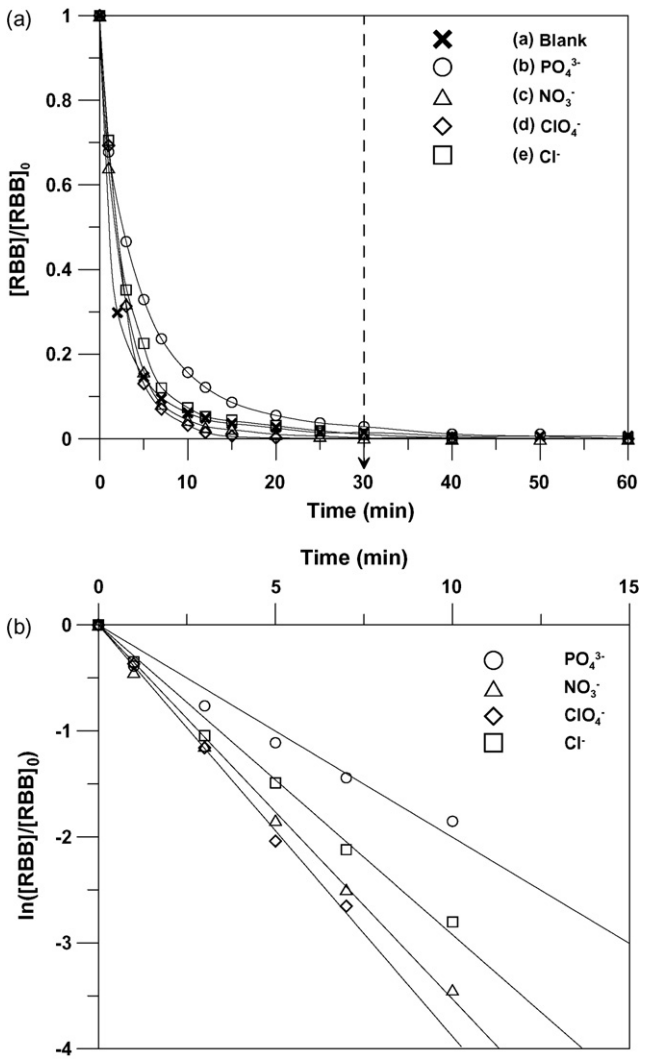

Fig. 6. Influences of various anions (10 mM) include chloride, perchlorate, nitrate, and phosphate on RBB removal during Co^{2+}/PMS oxidative processes (a); and kinetic plot of k_{obs} related to various ion effect (b). Experimental conditions: $[RBB]_0$ = 0.01 mM (10 ppm); $[Co^{2+}]_0 = 1.7 \times 10^{-3}$ mM (10 ppb); $[PMS]_0$ = 0.16 mM (100 ppm); reaction pH 6.0 (adjusted by $NaOH_{(aq)}$); reaction temperature = 25 °C.

experiment data used in Fig. 6b were selected within 10–15 min in order to have good correspondence with the comparison above. Consequently, the pseudo-first-order rate constants (k_{obs}) of RBB degradation were found to be 0.37 min^{-1} (R^2 = 0.91) with no anion addition, 0.31 min^{-1} (R^2 = 0.99) with 10 mM Cl^- addition, 0.39 min^{-1} (R^2 = 0.99) with 10 mM ClO_4^- addition, 0.36 min^{-1} (R^2 = 0.99) with 10 mM NO_3^- addition, and 0.22 min^{-1} (R^2 = 0.96) with 10 mM PO_4^- addition, respectively.

3.4. UV–vis spectra vicissitude of the RBB oxidization

To try to find out the possible interactions or to study the relationship between the decolorization and the decomposition of RBB, UV–visible absorption spectra of 0.1 mM RBB were practiced in this Co^{2+}/PMS oxidative process using a UV photo-diode array analyser (Fig. 7). All absorption spectra of RBB vicissitude during the Co^{2+}/PMS oxidative processes were accurately obtained from subtracting a background value of the single mixture of Co^{2+}/PMS from total absorption immediately with the UV analyser (λ = 190–1100 nm), thus also preventing further reactions. It can be seen in Fig. 7 that there are two main characteristic absorption bands of RBB vicissitude before and during treatment. One is in UV region (310 nm), and another is in the visible region (591 nm), and no absorbance was present as λ > 760 nm (i.e. infrared waves range). The UV band is characteristic of two adjacent rings, whereas the visible band is due to the long conjugated π system linked by two azo groups [28]. When comparing Fig. 7a–b with Fig. 3, it can be seen that not only the decolorization (591 nm) but also the information regarding aromatic fragment degradation (310 nm) can be determined. It is obvious both in Fig. 7a and b that the decline rate of the absorption peak in the visible region (591 nm) is much faster than that in the UV band region (310 nm), indicating bleaching of RBB (i.e. RBB degradation) is much easier than the decomposition of its aromatic fragment (i.e. intermediates degradation).

Both the decolorization rate (591 nm) and the degradation rate of the aromatic fragment (310 nm) increase efficiently as the Co^{2+}-catalyst dosage is increased from 1.7×10^{-4} mM (1 ppb) to 1.7×10^{-3} mM (10 ppb) in this phosphate buffered Co^{2+}/PMS process (pH 6). This observation is similar to that of $NaOH_{(aq)}$-adjusted processes as described in Figs. 4 and 5. When comparing Fig. 7a with Fig. 7b, it can be seen that the time consumption of complete decolorization can be greatly improved in the shrinkage from ">60 min" to "< 15 min" with a 1.7×10^{-3} mM (10 ppb) Co^{2+}-catalyst addition. Corresponding to Fig. 7a–b, Fig. 7c shows an absolute transparency of the reaction solution similar to clear water at least through 60 min, but it took only 15 min, as can be seen in Fig. 7d. This is due to the fact that the visible region (300–760 nm) is fortuitously the same as the development region of a camera, involving the chromophoric wavelength = 591 nm of the developed dye-RBB.

3.5. Bleaching and aromatic fragment degradation

In order to get a clear comparison between bleaching rates (591 nm) and the degradation of the aromatic fragment (310 nm), the absorbance of 0.01 mM RBB solution at 591 nm and 310 nm, as a function of time, was also measured in the Co^{2+}/PMS oxidative process. Fig. 8a–b shows a kinetic illustration intercepted from the 3D profile of phosphate-buffered RBB/Co^{2+}/PMS oxidative processes (Fig. 7a–b) at 591 nm and 310 nm, simultaneously. In comparison, the result of 591 nm in Fig. 8b (i.e. phosphate-buffered process) displays a much superior bleaching efficiency than that of the $NaOH_{(aq)}$-adjusted process with a 10 mM PO_4^{3-} addition (curve b in Fig. 6) but is very close to that of curve a in Fig. 6 (i.e. $NaOH_{(aq)}$-adjusted process with no anions addition). This indicates that no significant "ion effect" occurred, and no worse RBB decolorization resulted in the presence of 0.305 mM PO_4^{3-} as a buffered process. However, the performance became worse in that an "ion effect" occurred if the amount of anion species (i.e. PO_4^{3-}) was increased to a certain concentration of 10 mM, such as a 33-flod overdose (i.e. curve b in Fig. 6).

The produced radicals ($SO_4^{-\bullet}$ and $^\bullet OH$) would rather first attack azo groups and open the N=N bonds, destroying the long conjugated π systems, and consequently causing decolorization. Owing to the fact that N=N bonds are much easier to destroy than aromatic ring structures, the elimination of adjacent ring structures takes a longer time as can be seen and is totally be supported from Fig. 8. In addition, it is worth mentioning that no growth and/or accumulation of aromatic ring structures (i.e. 310 nm) can be observed, indicating that this expected Co^{2+}/PMS process has a powerful oxidative ability for not only a complete decolorization but also a continuous destruction of aromatic intermediates. Even a total aromatic decomposition may be achieved if there is a much longer period of contact or conjunction with other treatments of AOPs in this optimum situation.

Similar to the suggested two-stage hypothesis, the Fenton reaction stage (Fe^{2+}/H_2O_2) and Fenton-like reaction stage (Fe^{3+}/H_2O_2) in Fenton processes [1], the observations in Fig. 8 support that the

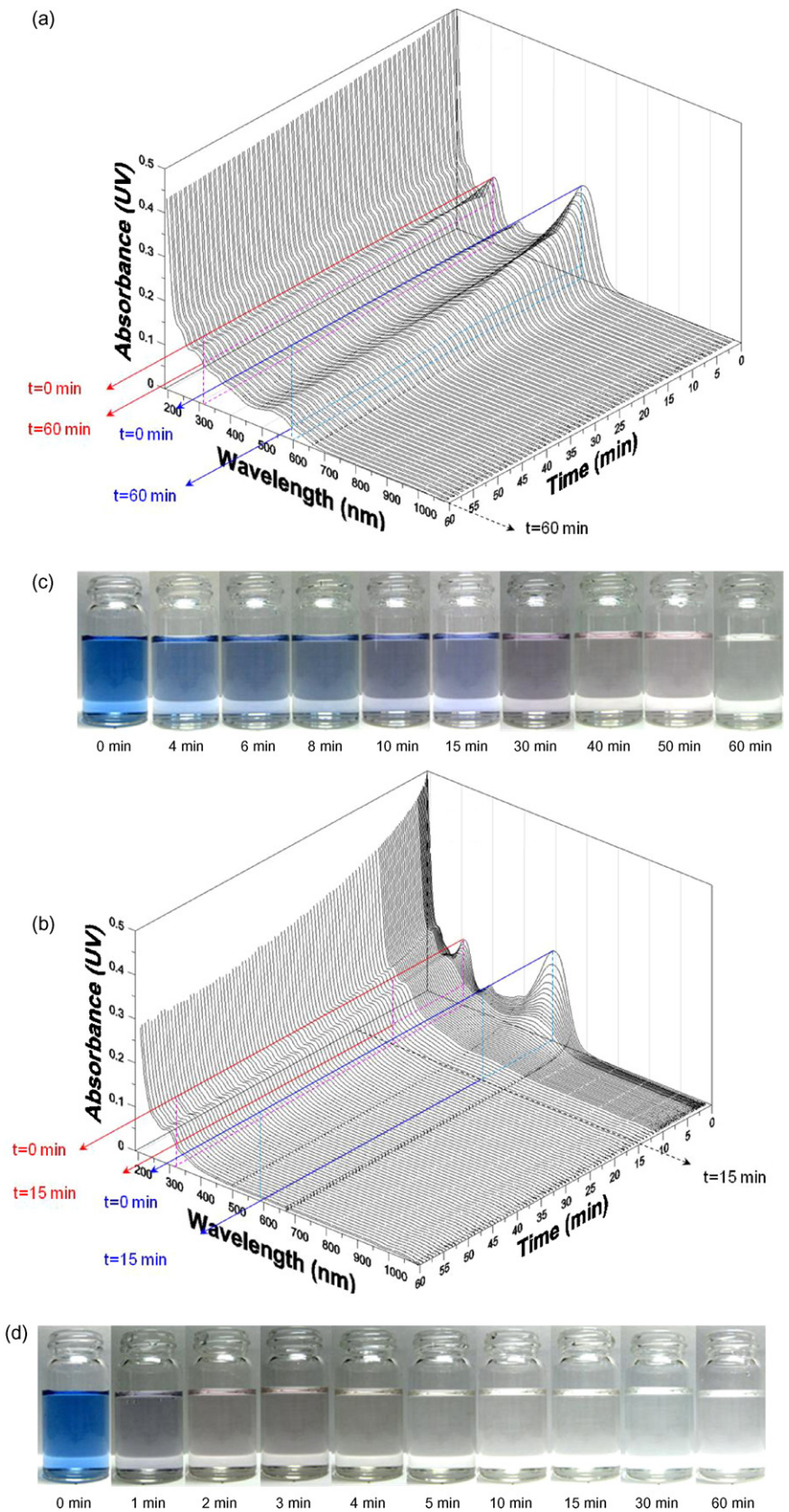

Fig. 7. UV–vis absorption spectra of RBB and its derivatives during degradation with 1.7×10^{-4} mM (1 ppb) Co^{2+}-catalyst (a) or with 1.7×10^{-3} mM (10 ppb) Co^{2+}-catalyst (b); and the photos of RBB decolorization correspond to reaction time with 1.7×10^{-4} mM (1 ppb) Co^{2+}-catalyst (c) or with 1.7×10^{-3} mM (10 ppb) Co^{2+}-catalyst (d) in this buffered Co^{2+}/PMS process as comparative study. Experimental conditions: $[RBB]_0 = 0.01$ mM (10 ppm); $[PMS]_0 = 0.16$ mM (100 ppm); reaction was buffered at pH 6.0 by 0.305 mM PO_4^{3-}; reaction temperature = 25 °C.

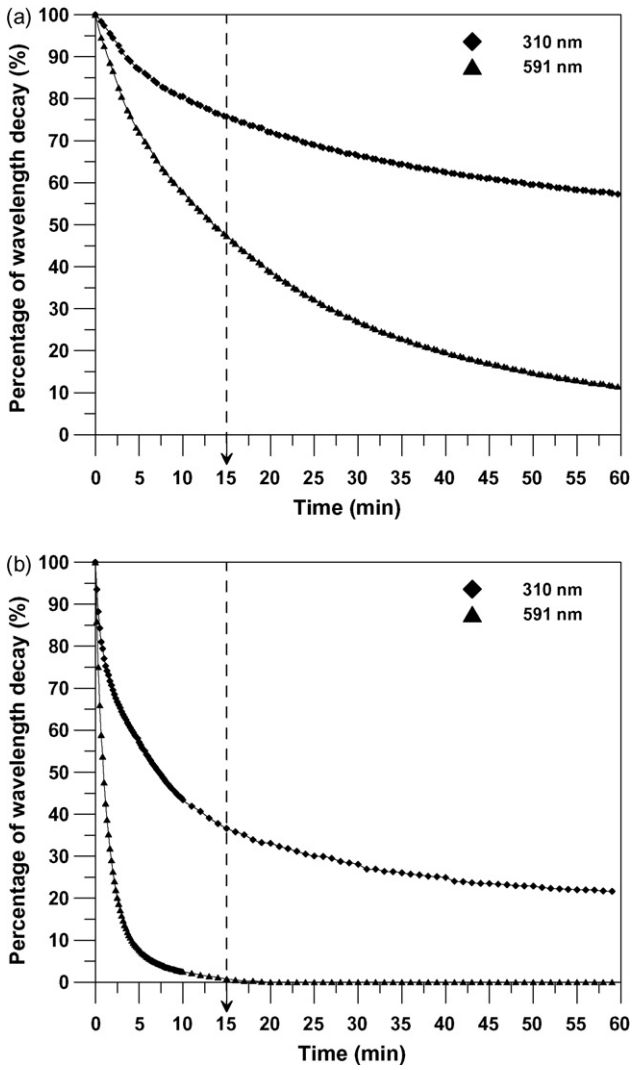

Fig. 8. Comparison between the decolorization at 591 nm (i.e. RBB removal) and aromatic fragment degradation at 310 nm from the 0.01 mM RBB solution during the buffered Co^{2+}/PMS oxidative process. Experimental conditions: $[RBB]_0 = 0.01$ mM (10 ppm); $[PMS]_0 = 0.16$ mM (100 ppm); $[Co^{2+}]_0 = 1.7 \times 10^{-4}$ mM (1 ppb) (a) and $[Co^{2+}]_0 = 1.7 \times 10^{-3}$ mM (10 ppb) (b); reaction was buffered at pH 6.0 by 0.305 mM PO_4^{3-}; reaction temperature = 25 °C.

Co^{2+}/PMS process could theoretically be divided into two stages, too. This is especially evident in Fig. 8b, which shows that both the plots of 591 nm and 310 nm indicate a high declination rate in the first 10–15 min, followed by a slower variation. The points of inflexion might indicate the separation between the following two different reaction stages, the Co^{2+}-activated reaction stage and the Co^{3+}-activated reaction stage, sequentially:

$$Co^{2+} + HSO_5^- \text{ or } HSO_4^- \rightarrow Co^{3+} + (HO^- + SO_4^{-\bullet} \text{ or } SO_3^{-\bullet}) \text{ or } (HO^\bullet + SO_4^{2-} \text{ or } SO_3^{2-}) \quad (5)$$

$$Co^{3+} + HSO_5^- \text{ or } HSO_4^- \rightarrow Co^{2+} + SO_5^{-\bullet} \text{ or } SO_4^{-\bullet} + H^+ \quad (6)$$

In the first stage, the azo bonds of RBB decomposed very quickly due to the high reactivity with powerful radicals ($SO_4^{-\bullet}$ or $SO_3^{-\bullet}$ or $^\bullet OH$) produced from the reaction between Co^{2+} ions and PMS (Eq. (5)), resulting in a sharp decline of wavelength color (591 nm) as shown in Fig. 8b. The Co^{3+} ions generated from Eq. (5) can react with residual PMS (i.e. HSO_5^- or HSO_4^-) to produce additional $SO_4^{-\bullet}$ radicals (or $SO_5^{-\bullet}$) and also to regenerate Co^{2+} ions, performed as the second reaction stage (Eq. (6)). Although the regenerated reagent (i.e. Co^{2+}) from Eq. (6) could further react with the remaining PMS solution to continue dye degradation, the oxidation rate of this second stage was slower than the first stage due to slow transformation of Co^{3+} to Co^{2+}.

However the tendency of absorbance decline rate and the inflexion is not obvious in Fig. 8a; this is probably due to the fact that the participation of the initial Co^{2+} concentration was relatively and significantly lower than that applied in Fig. 8b, leading to an insufficient amount of the Co(II,III)-catalyst (Eqs. (5), (16)–(17)) to continuously activate the 100 ppm PMS efficiently via the chain oxidative pathways suggested in Section 3.6. The above result has a good correspondence with Section 3.2 that the ideal dosage of Co^{2+} for actual application is 10 ppb.

3.6. Possible chain oxidative pathways of RBB

The metal-ions (i.e. Co(II,III)) used throughout this work do not absorb the UV radiation in the visible region (300–760 nm), as is the case when coabsorbance occurred with PMS only at wavelengths below 300 nm. Hence, the main absorbing species is the RBB (see Fig. 7).

In response to the result stated in above section, RBB is shown not to be completely decomposed in a 1 ppb Co^{2+}-catalytic solution, but in a 10 ppb Co^{2+}-catalytic solution, a much longer contact time (>60 min) is needed. It can be concluded that during the first 10 min (i.e. the first stage; Eq. (5)), the PMS acts as the dominant oxidant in solution (see Fig. 8b). Besides the circulating Co^{2+} regenerated as a second reaction stage (Eq. (6)), the formation of peroxides ($ROO^\bullet$) in this stage also contributes in an important pathway to the decomposition (or partial mineralization) of RBB [29,30]. Consequently, based on this work and a related literature review [12,17,31], the possible chain oxidative pathways for the degradation of RBB with Co^{2+} and PMS can be simply generalized and suggested below to describe the oxidation of RBB (Eqs. (7)–(14)):

$$RBB + Co^{2+} \rightarrow [RBB\cdots Co^{2+}] \quad (7)$$

The hydrolysis equilibrium [32,33] of HSO_5^- is also reported to take place in neutral conditions [34] as represented by Eq. (8) as follows:

$$HSO_5^- + H_2O \leftrightarrow H_2O_2 + HSO_4^- \quad (8)$$

$$[RBB\cdots Co^{2+}] + HSO_5^- \text{ or } HSO_4^- \rightarrow\rightarrow RBB^{+\bullet} + Co^{2+} + (HO^- + SO_4^{-\bullet} \text{ or } SO_3^{-\bullet}) \quad (9)$$

As an organics-selective-oxidant that differs from $^\bullet OH$, $SO_4^{-\bullet}$ would prefer to attack aromatic compounds first, thus benefiting the decomposition of both RBB and its derivative aromatic fragments:

$$RBB^{+\bullet} + HSO_5^- \text{ or } HSO_4^- \rightarrow [\text{organics (HR)}] + (HO^- + SO_4^{-\bullet} \text{ or } SO_3^{-\bullet}) \quad (10)$$

$$Co^{2+} + HSO_5^- \text{ or } HSO_4^- \rightarrow Co^{3+} + (HO^- + SO_4^{-\bullet} \text{ or } SO_3^{-\bullet}) \text{ or } (HO^\bullet + SO_4^{2-} \text{ or } SO_3^{2-}) \quad (11)$$

$$RBB^{+\bullet} + Co^{2+} \text{ or } Co^{3+} \rightarrow \text{organics} + Co^{2+} \text{ or } Co^{3+} \quad (12)$$

$$\text{Organics} + HO^\bullet + SO_4^\bullet \text{ or } SO_3^\bullet \rightarrow [\text{radical intermediates}(R^\bullet)] \quad (13)$$

The metal-catalyzed autoxidation of the (bi)sulfite anion, studied for decades, is also proposed to be an oxygen-consuming chain reaction [35–37], including:

$$R^{\bullet} + (HSO_5^- \text{ or } HSO_4^-)/O_2 \rightarrow \text{organics} \rightarrow CO_2 + H_2O \quad (14)$$

The possible side reactions and the Co^{2+} (i.e. divalent metals) regeneration [12,17,31] are suggested below, thereby progressing the efficient activation of PMS and degradation of RBB continuously even with an extremely low dosage of $[Co^{2+}]_0 = 1–10\ \mu g\ L^{-1}$:

$$HSO_5^- \text{ or } HSO_4^- + (SO_4^{-\bullet} \text{ or } SO_3^{-\bullet} \text{ or } HO^{\bullet}) \rightarrow SO_5^{-\bullet} \text{ or } SO_4^{-\bullet} + (SO_4^{2-} \text{ or } SO_3^{2-} \text{ or } HO^-) + H^+ \quad (15)$$

$$Co^{3+} + HSO_5^- \text{ or } HSO_4^- \rightarrow Co^{2+} + SO_5^{-\bullet} \text{ or } SO_4^{-\bullet} + H^+ \quad (16)$$

$$R^{\bullet} + O_2 \rightarrow ROO^{\bullet} \xrightarrow{Co^{3+}} \text{oxygenated products} \rightarrow Co^{2+} + {}^{\bullet}OH \quad (17)$$

The dissolved O_2 may play an active role leading to the peroxy-radicals, $ROO^{\bullet}$ (R = H, alkyl, aryl) [38,39], and $ROO^{\bullet}$ will serve as chain propagators and will oxidize organic materials either by hydrogen abstraction or by an electron transfer process [40,41]. Thereby, there is even a definite opportunity for it to further collide with another radical intermediate ($R^{\bullet}$ or $ROO^{\bullet}$) to yield a macromolecule [18]:

$$ROO^{\bullet} \text{ or } R^{\bullet} + (ROO^{\bullet} \text{ or } R^{\bullet}) \rightarrow \text{macromolecular organics} \quad (18)$$

4. Conclusions

The decolorization and degradation of RBB were successfully performed using sulfate and hydroxyl radicals generated by the conjunction of peroxymonosulfate with an extremely low dosage of cobalt catalyst (Co^{2+}/PMS) in neutral pH conditions. Only a molar ratio of $[PMS]_0/[RBB]_0 = 8–32$ and a minimum dosage of $[Co^{2+}]_0 = 1–10$ ppb were utilized. The experimental results showed that the use of this Co^{2+}/PMS oxidative process without any photo-promotion is very beneficial to not only the complete decolorization of RBB but also to the degradation efficiency of its derivative aromatic fragments. Fortunately, this expected low dosage Co^{2+}/PMS oxidative process can be seen as a superior choice as a good pretreatment to selectively decompose the stubborn structure of benzenic and phenolic derivatives first although a low mineralization efficiency is the common drawback of a single use of the sulfite–bisulfite–pyrosulfite systems. Consequently, facilitating the mineralization for the follow-up treatment of other AOPs through this Co^{2+}/PMS oxidative process is expected as can be seen in the results of this work. The anion effects were further carried out successfully not only to simulate a textile waste stream but also to prove the high oxidative ability of this Co^{2+}/PMS process even in a phosphate-buffered solution, where, in spite of the negative effect, it can be totally overcome.

Acknowledgements

The authors would like to thank the National Science Council of the Republic of China, Taiwan, for financially supporting this research under Contract No. NSC 97–2221–E–006–042.

References

[1] M.S. Lucas, J.A. Peres, Decolorization of the azo dye reactive Black 5 by Fenton and photo-Fenton oxidation, Dyes Pigments 71 (2006) 236–244.
[2] Y.H. Huang, Y.F. Huang, P.S. Chang, C.Y. Chen, Comparative study of oxidation of dye-Reactive Black B by different advanced oxidation processes: Fenton, electro-Fenton and photo-Fenton, J. Hazard. Mater. 154 (2008) 655–662.
[3] S.F. Kang, C.H. Liao, M.C. Chen, Pre-oxidation and coagulation of textile wastewater by the Fenton process, Chemosphere 46 (2002) 923–928.
[4] S. Anandan, Photocatalytic effects of titania supported nanoporous MCM-41 on degradation of methyl orange in the presence of electron acceptors, Dyes Pigments 76 (2008) 535–541.
[5] J.H. Sun, S.P. Sun, G.L. Wang, L.P. Qiao, Degradation of azo dye Amido black 10B in aqueous solution by Fenton oxidation process, Dyes Pigments 74 (2007) 647–652.
[6] W.P. Ting, Y.H. Huang, M.C. Lu, Catalytic treatment of petrochemical wastewater by electroassisted Fenton technologies, React. Kinet. Catal. Lett. 92 (2007) 41–48.
[7] M.D.A. Khan, R.J. Watts, Mineral-catalyzed peroxidation of tetrachloroethylene, Water Air Soil Pollut. 88 (1996) 247–260.
[8] M. Kitis, C.D. Adams, G.T. Daigger, The effects of Fenton's reagent pretreatment on the biodegradability of nonionic surfactans, Water Res. 33 (1999) 2561–2568.
[9] M.C. Lu, C.J. Lin, C.H. Liao, W.P. Ting, R.Y. Huang, Influence of pH on the dewatering of activated sludge by Fenton's reagent, Water Sci. Technol. 44 (2001) 327–332.
[10] E. Neyens, J. Baeyens, A review of classic Fenton's peroxidation as an advanced oxidation technique, J. Hazard. Mater. B98 (2003) 33–50.
[11] C. Walling, Fenton's reagent revisited, Acc. Chem. Res. 8 (1975) 125–131.
[12] Y.H. Huang, S.T. Tsai, Y.F. Huang, C.Y. Chen, Degradation of commercial azo dye reactive Black B in photo/ferrioxalate system, J. Hazard. Mater. 140 (2007) 382–388.
[13] S. Tanaka, M. Kawai, Y. Nakata, M. Terashima, H. Kuramitz, M. Fukushima, Degradation of bisphenol A by photo-fenton processes, Toxicol. Environ. Chem. 85 (2003) 95–102.
[14] Y.F. Huang, Y.H. Huang, Identification of produced powerful radicals involved in the mineralization of Bisphenol A using a novel UV-$Na_2S_2O_8$/H_2O_2-Fe(II,III) two-stage oxidation process, J. Hazard. Mater. 162 (2009) 1211–1216.
[15] T. Pandurengan, P. Maruthamuthu, Kinetics and mechanism of oxidation of dimethyl sulfoxide by peroxomonosulfate, B. Chem. Soc. Jpn. 54 (1981) 3551–3555.
[16] R. Renganathan, P. Maruthamuthu, Kinetics and mechanism of oxidation of aliphatic aldehydes by peroxomonosulphate, Int. J. Chem. Kinet. 18 (1986) 49–58.
[17] G.P. Anipsitakis, D.D. Dionysiou, Transition metal/UV-based advanced oxidation technologies for water decontamination, Appl. Catal. B-Environ. 54 (2004) 155–163.
[18] G. Manivannan, P. Maruthamuthu, Peroxo salts as initiators of vinyl polymerization-III. Polymerization of acrylonitrile initiated by the peroxomonosulphate-Co(II) redox system, Eur. Polym. J. 23 (1987) 311–313.
[19] C. Cuypers, T. Grotenhuis, K.G.J. Nierop, E.M. Franco, A.D. Jager, W. Rulkens, Amorphous and condensed organic matter domains: the effect of persulfate oxidation on the composition of soil/sediment organic matter, Chemosphere 48 (2002) 919–931.
[20] G.H. Scott, E.P. Bruce, In-Situ Chemical Oxidation-Engineering Issue, Ground Water and Ecosystem Restoration Information Center, UAEPA, EPA/600/R-06/072, 2006, http://www.epa.gov/ada/download/issue/600R06072.pdf.
[21] G.R. Peyton, The free-radical chemistry of persulfate-based total organic carbon analyzers, Mar. Chem. 41 (1993) 91–103.
[22] X.Y. Yu, Z.C. Bao, J.R. Barker, Free radical reactions involving $Cl^{\bullet}$, $Cl_2^{-\bullet}$, and $SO_4^{-\bullet}$ in the 248 nm photolysis of aqueous solutions containing $S_2O_8^{2-}$ and Cl^-, J. Phys. Chem. A 108 (2004) 295–308.
[23] Y.F. Huang, Y.H. Huang, Behavioral evidence of the dominant radicals and intermediates involved in Bisphenol A degradation using an efficient Co^{2+}/PMS oxidation process, J. Hazard. Mater. Accepted Manuscript, available online 14 January (2009), in Press.
[24] J.W.T. Spinks, R.J. Woods, An Introduction to Radiation Chemistry, 3rd ed., John Wiley & Sons, New York, 1990.
[25] T. Ernst, M. Wawrenczyk, M. Cyfert, M. Wronska, Effect of pH on the kinetics of ferrate(VI) decomposition, Bull. Acad. Pol. Sci. Ser. Sci. Chim. 27 (1979) 773–778.
[26] M. Muruganandham, M. Swaminathan, Photochemical oxidation of reactive azo dye with UV-H_2O_2 process, Dyes Pigments 62 (2004) 269–275.
[27] E. Sato, M. Kato, M. Kohno, Y. Niwano, Clindamycin phosphate scavenges hydroxyl radical, Int. J. Dermatol. 46 (2007) 1185–1187.
[28] R.M.C. Silverstein, G.C. Basdler, G.C. Morrill, Spectrophotometric Identification of Organic Compounds, Wiley, New York, 1991.
[29] J. Fernandez, P. Maruthamuthu, J. Kiwi, Photobleaching and mineralization of Orange II by oxone and metal-ions involving Fenton-like chemistry under visible light, J. Photoch. Photobio. A 161 (2004) 185–192.
[30] J. Fernandez, P. Maruthamuthu, A. Renken, J. Kiwi, Bleaching and photobleaching of Orange II within seconds by the oxone/Co2 + reagent in Fenton-like processes, Appl. Catal. B: Environ. 49 (2004) 207–215.
[31] G.P. Anipsitakis, D.D. Dionysiou, Degradation of organic contaminants in water with sulfate radicals generated by the conjunction of peroxymonosulfate with cobalt, Environ. Sci. Technol. 37 (2003) 4790–4797.
[32] S. Dubey, S. Hemkar, C.L. Khandelwal, P.D. Sharma, Kinetics and mechanism of oxidation of hypophosphorous acid by peroxomonosulphate in acid aqueous medium, Inorg. Chem. Commun. 5 (2002) 903–908.
[33] D.L. Ball, J.O. Edwards, The kinetics and mechanism of the decomposition of Caro's Acid. I, J. Am. Chem. Soc. 78 (1956) 1125–1129.
[34] J. Balej, Thermodynamics of reactions during the electrosynthesis of peroxodisulphates, Electrochim. Acta 29 (1984) 1239–1242.
[35] E. Hayon, A. Treinin, J. Wilf, Electronic spectra, photochemistry, and autoxidation mechanism of the sulfite-bisulfite-pyrosulfite systems. SO_2^-, SO_3^-, SO_4^-, and SO_5^- radicals, J. Am. Chem. Soc. 94 (1972) 47–57.

[36] J.M. McCord, I. Fridovich, The utility of superoxide dismutase in studying free radical reactions, J. Biol. Chem. 244 (1969) 6056–6063.
[37] G.A. Reed, J.F. Curtis, C. Mottley, T.E. Eling, R.P. Mason, Epoxidation of (±)-7,8-dihydroxy-7,8-dihydrobenzo[α]pyrene during (bi)sulfite autoxidation: Activation of a procarcinogen by a cocarcinogen, P. Natl. Acad. Sci. USA 83 (1986) 7499–7502.
[38] V. Nadtochenko, J. Kiwi, Photoinduced adduct formation between Orange II and [Fe^{3+}(aq)] or $Fe(ox)_3^{3-}$–H_2O_2 photocatalytic degradation and laser spectroscopy, J. Chem. Soc. Faraday T. 93 (1997) 2373–2378.
[39] B. Ruppert, R. Bauer, G. Heisler, The photo-Fenton reaction – an effective photochemical waste-water treatment process, J. Photoch. Photobio. A 73 (1993) 75–78.
[40] K.U. Ingold, Peroxy radicals, Accounts Chem. Res. 2 (1969) 1–9.
[41] B. Maillard, K.U. Ingold, J.C. Scaiano, Rate constants for the reactions of free radicals with oxygen in solution, J. Am. Chem. Soc. 105 (1983) 5095–5099.